To demonstrate this, first notice that $|e^{i(\delta+\bar{\delta})}| = 1$. This follows from the fact that

$$e^{i(\delta+\bar{\delta})} \cdot [e^{i(\delta+\bar{\delta})}]^* = [e^{i\delta}\{e^{i\bar{\delta}}\}^*] \cdot [e^{i\bar{\delta}}\{e^{i\delta}\}^*],$$

and each of these factors has the form of the middle term of (13), where a is not required to be real for the second equality to hold.

Now $e^{i(\delta+\bar{\delta})}$ can be expressed with real coefficients as

$$e^{i(\delta+\bar{\delta})} = \frac{(r+\sqrt{r^2-1})e^{i\phi} - 2\alpha/r + (r-\sqrt{r^2-1})e^{-i\phi}}{2\sqrt{x^2-2\alpha x+\alpha^2+\beta^2}}, \quad (18)$$

where r is defined as the semi-major axis of the ellipse passing through (α, β) with foci at ± 1.[18] The quantities under the radical signs are all positive so that (18) is well defined and valid for all α if $\beta \neq 0$. If $\beta = 0$ and $\alpha > 1$ then (17) reduces to (11) and if $\alpha < 1$, (17) reduces to the square of (13). Finally

$$\sin(\delta+\bar{\delta}) = \frac{\sqrt{r^2-1}\sin\phi}{2\sqrt{x^2-2\alpha x+\alpha^2+\beta^2}}$$

so that $\delta+\bar{\delta}$ goes from 0 to π as ϕ does since $\sin(\delta+\bar{\delta})$ is positive everywhere in between, regardless of the sign of α.

[18] For the transformations involved see Bernstein.[15]

ACKNOWLEDGMENT

The author wishes to thank J. Nardi, now at the Brookhaven National Laboratory, who made the numerical calculations and measurements reported and whose determination of several equal-ripple functions by the potential analog method suggested the general solution which is the basis for this paper.

A Broad Tunable Bandwidth Traveling-Wave Maser

L. C. MORRIS, MEMBER, IEEE, AND D. J. MILLER, MEMBER, IEEE

Summary—**A new type of traveling-wave maser (TWM) has been developed, employing the meander line as the slow-wave circuit and rutile as the active maser crystal. This amplifier has achieved net gains in excess of 23 db across the band from 2.0 to 3.0 Gc, with an over-all noise temperature of 8°±2°K. This marks the first time that rutile with a dielectric constant of 220 has been coupled to a slow-wave circuit. The maser material exhibited inversion ratios of 10:1 and saturated at an input signal of −47 dbm. In addition to the maser work, a ferrite material investigation was conducted, which led to the development of a gadolinium substituted yttrium iron garnet (YIG) as the ferrite isolator. Various concentrations of the gadolinium in YIG were investigated as ferrite isolators at 4.2°K and were found to have lower forward losses than pure YIG at *S* band.**

INTRODUCTION

THE THEORY and advantages of the traveling-wave maser over the cavity maser has been well established and given in the literature [1], [2]. Various slow-wave structures, such as the comb structure [1], Karp structure [3], meander line [4]–[6] and the dielectrically loaded waveguides [7], have been used to obtain the low group velocities necessary for traveling-wave maser action. This paper specifically describes the design of an *S*-band rutile loaded meander line. The energy levels and crystal axis orientations of rutile are discussed since this is the first time this material has been used at such low frequencies.

The initial desire for a large tunable bandwidth eliminated structures such as the comb and Karp because of their highly resonant, narrow bandwidth characteristics. A slow-wave structure which exhibited wide dispersion characteristics, relatively low impedance variations as a function of frequency and low insertion losses was needed. Investigations showed the meander line to possess these characteristics.

Rutile was selected as the active paramagnetic material because of its very high inversion ratio, high dielectric constant, high signal power saturation levels and the ability to obtain large single crystals with accurate crystal axis alignment.

CHARACTERISTICS OF RUTILE [8]

Ruby has been generally used as the active material in TWM's. For this application, certain improved characteristics were desired, and rutile was considered as superior to ruby for TWM design. The pertinent characteristics of these two materials are compared in Table I. Note the advantages of rutile's lower Q_m and higher dielectric constant. Also, the zero field splitting for rutile is large, which contributes to a higher inversion ratio. In addition rutile saturates at a relatively high input level. Rutile was selected for these advantages,

Manuscript received November 4, 1963; revised March 16, 1964.
The authors are with the Radio Corporation of America, Camden, N. J.

plus the ability to grow large single crystals, maintain accurate crystal axis alignment and provide uniform doping concentration; rutile can also amplify over a large microwave spectrum.

Note 1: These values of Q_m are for comb and meander line traveling-wave masers loaded with active material on one side of the finger only.

The host crystal, titania (TiO_2), is a very hard crystal and withstands large temperature changes. Its crystal structure is tetrahedral (D_{4h}). The dielectric constant of titania is very large (121 perpendicular and 220 parallel to the c axis at 4.2°K) [9].

When chromium is added to the titania crystal, the material becomes black and the crystal axes must be found by X-ray analysis. Fig. 1 shows the crystal axes and their related magnetic axes. The magnetic axes and the crystal field parameters, and their related direction cosines, are shown below.

TABLE I
CHARACTERISTICS OF RUBY AND RUTILE

Characteristic	Ruby Al_2O_3	Rutile TiO_2
Zero Field Splitting	12 Gc	43.3 Gc
Spin Density	10^{19} spins/cc	10^{19} spins/cc
Input Saturation Level	−65 dbm	−47 dbm
Dielectric Constants	12	110 220
Line Width	58 Mc	30 Mc
Q_m (Note 1)	150	50
Inversion Ratio	4:1 (S band)	10:1 (S band)

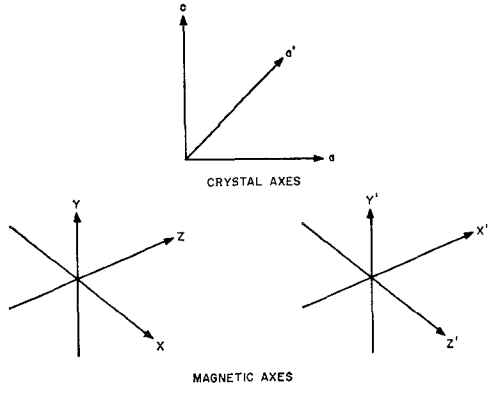

Fig. 1—Crystal and magnetic axes of chromium-doped titania.

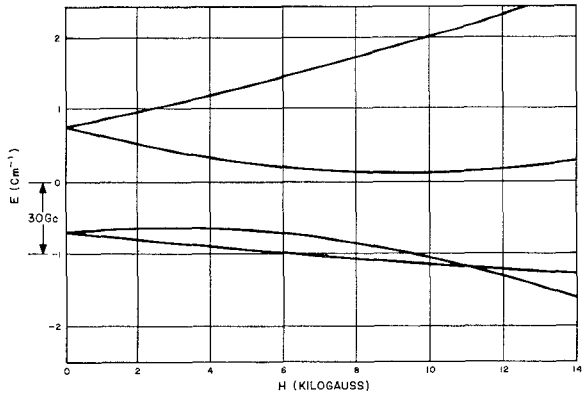

Fig. 2—Y-axis energy levels for chromium-doped rutile.

There are two titanium (or chromium) ions per unit cell (double-ion site), related by a 90° rotation about the Y axis. Masers can be operated in this double-ion site where both chromium ions per unit cell are acted on simultaneously; this will double the normal gain. Fig. 2 shows the Y-axis (double ion site) energy level employed throughout this work. Crystals were grown with a chromium concentration of 0.05 per cent by weight Cr_2O_3, which is equivalent to 0.0342 per cent by weight Cr^{+3}, or 342 ppm. A boule with a 2.5-mm longitudinal slice taken through the middle was analyzed every $\frac{1}{16}$ inch over a length of 3 inches; the results showed a concentration of 139 ppm minimum to 230 ppm maximum.

Meander Line Characteristics

The meander line (Fig. 3), basically employs geometrical slowing. Geometrical slowing is, in its simplest form, the ratio of the actual path length to the net axial length of the circuit. The tape meander line, first proposed as a maser structure by Siegman [6] and analyzed by Butcher [10], [11], was selected for this application because of its wide dispersion characteristics, its ease of fabrication and its reasonable circuit dimensions. As a first order approximation, slowing in the meander line can be expressed as

$$S = 2(1 + a/b)\sqrt{\epsilon'} \tag{1}$$

where ϵ' is the effective dielectric constant of the maser crystal, not to be confused with the measured values shown in Table I, and dimensions a and b are as shown in Fig. 3.

Typical values of ϵ' are on the order of 6. Note that this expression for slowing does not account for the changes in the value of slowing with changing frequency and represents a first-order approximation based on geometrical factors only.

The structure supports transverse electromagnetic (TEM) waves for tape widths of approximately a quarter wavelength. These TEM waves can be envisioned as traveling back and forth along the tapes at right angles to the slow-wave direction of propagation. This in reality amounts to a mixture of resonant and geometrical slowing.

The ratio of the air gap width to the copper width is a critical parameter, since it directly influences the dispersion characteristic or slowing. For the limiting case of a small copper width and a large air gap, the circuit wave follows the copper at the velocity of light, resulting in the linear curve which is characteristic of pure geometrical slowing. When the air gap is narrowed, the ω-β curve departs from linearity and exhibits the properties of resonant slowing. An attractive feature of the meander line is the broad middle range of the ω-β curve, which permits maser operation with good slowing over a wide frequency tuning range. The tunable band can be achieved by adjusting the copper-to-air ratio.

When rutile, with its high dielectric constant and large inversion ratio, is coupled to this circuit, excellent gains are possible over a broad tunable range.

To substantiate this approach, a number of meander line circuits were experimentally evaluated for slowing.

The slowing curves shown in Fig. 4 were obtained by varying the copper-to-air ratio for a fixed meander line width of 0.600 inch. Since these curves are for unloaded lines, a dielectric coupling factor $\sqrt{\epsilon'}$ must be added to determine the true slowing value of the structure. Since the gain is directly proportional to slowing, the curves of Fig. 4 provide a direct indication of useful tunable bandwidth. The broadest bandwidth shown in these curves is achieved with a copper-to-air ratio of 1:1; increasing the ratio decreases the bandwidth, thereby increasing the peak values of slowing over a narrower bandwidth.

Note that the values of slowing shown by the curves of Fig. 4 are higher than indicated by the preceding approximate equation for slowing; this is primarily because of the partial resonance slowing which places the measured values of slowing within the usable tunable bandwidth above the average values calculated from (1). The Cooper to Air ratio of 1:1 was selected for the traveling-wave maser operating over the range from 2 to 3 Gc.

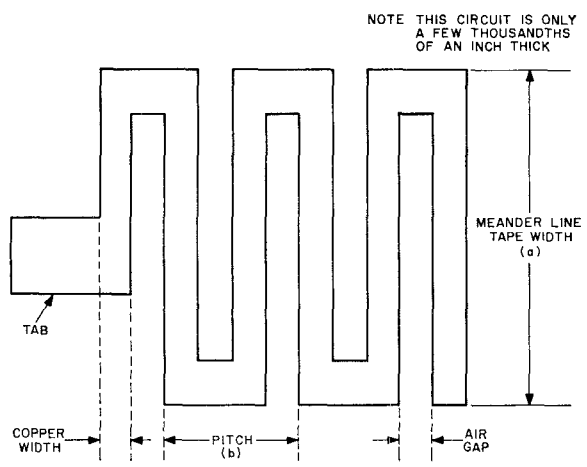

Fig. 3—Top view of meander line slow-wave circuit.

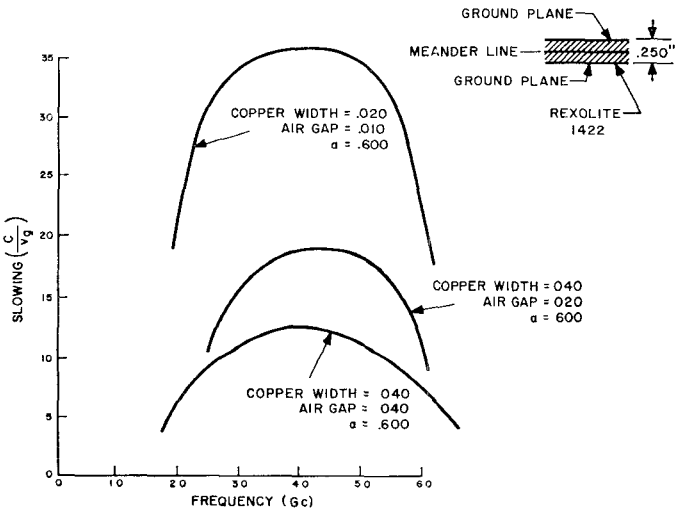

Fig. 4—Slowing vs frequency.

The structure pass band is determined by the meander line width, the pitch, the effective dielectric constant and the area covered by the maser crystal, or the filling factor. The meander line width (Fig. 3) can be computed approximately as

$$a = (\lambda/4)\sqrt{\epsilon'}. \tag{2}$$

Using a structure with 0.75 ratio of rutile width to meander line width, ϵ' was found experimentally to be 6.2. The rutile was located off the surface of the line, and the value of ϵ' depends on the exact spacing of the rutile from the surface of the meander line.

Ferrite Isolator

To meet the stringent amplifier stability requirements (short circuit gain stable), it is necessary to incorporate some form of reverse isolation into the circuit. This is accomplished by using a ferromagnetic material. Ferrites have much stronger resonances than paramagnetic materials and their optimum nonreciprocal polarization is circular. When the ferrite sample is properly shaped, the ferrite resonance will track the same dc field as needed for the maser crystal. These ferrites must operate at liquid helium temperatures and exhibit sufficient line width for tracking purposes.

The resonance frequency of a ferrite sample is determined by the dc magnetic field, the saturation magnetization ($4\pi M_s$) and the demagnetizing effect of the selected sample shape. These factors are described by the Kittel equation, which is plotted in Fig. 5.

$$f = \gamma\{[H_A - (N_Z - N_X)4\pi M_S] \cdot [H_A - (N_Z - N_y)4\pi M_S]\}^{1/2} \tag{3}$$

where

f = Resonance frequency in Mc.
γ = Gyromagnetic ratio (2.8 Mc per gauss for pure YIG).
H_A = Applied dc magnetic field.
$4\pi M_s$ = Magnetization, saturation value.
N_X, N_Y, and N_Z = Demagnetizing factors.

A reverse isolator utilizing pure YIG can be designed for rutile at S band. However, this requires that the YIG must be operated within or near the nonsaturated region, with a substantial penalty in insertion losses due to the forward losses of the ferrite. The problem of ferrite losses could be overcome, with a corresponding increase in net gain, if it were possible to find a new type of ferrite with a lower $4\pi M_s$. A variety of possible substituted YIG's were investigated, and it was concluded that gadolinium might prove a suitable material for this

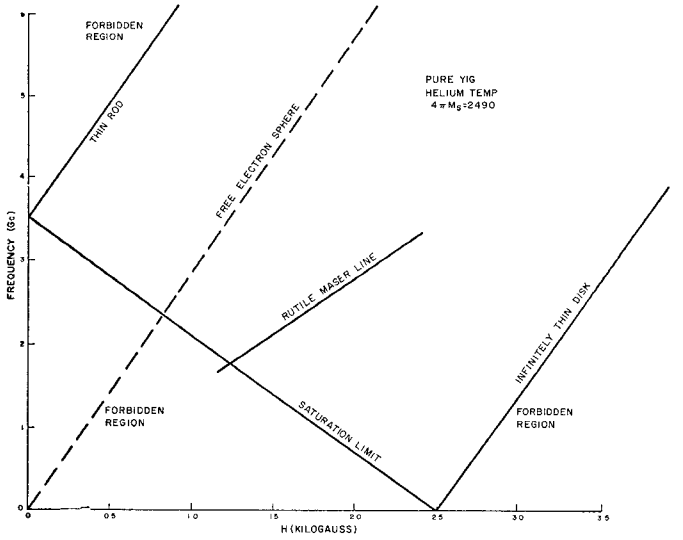

Fig. 5—Plot based on Kittel's equation.

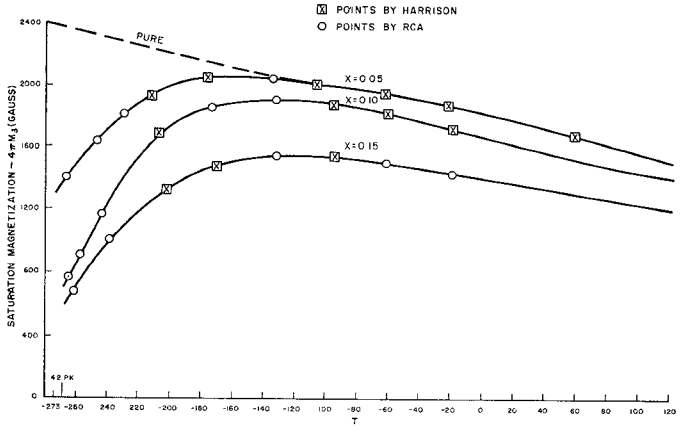

Fig. 6—Variation of $4\pi M_s$ with temperature for mixed gadolinium YIG.

TABLE II

FOWARD-TO-BACK RATIOS FOR PURE YIG AND DOPED YIG

Frequency (Gc)	Pure YIG Forward-to-back Ratio(db)	Gd-YIG (10 per cent) Forward-to-back Ratio (db)
2.0	10:1	25:1
2.1	10:1	40:1
2.2	10:1	
2.3	10:1	24:1
2.4	10:1	39:1
2.5	11:1	26:1
2.6	11:1	40:1
2.7	12:1	25:1
2.8	12:1	16:1
2.9	10:1	
3.0	14:1	23:1

purpose. Since none of the workers in the field had reported on the change in $4\pi M_s$ of polycrystalline gadolinium doped YIG at 4.2°K, the work started at this point by substituting the characteristics for 5, 10, and 15 per cent gadolinium into the following formula [12]:

$$3[(1.00 - X)Y_2O_3 \bullet XGd_2O_3].5F_2O_3 \qquad (4)$$

where X is the per cent substitution of the Gd ion. Using the same aspect ratio for all three substitutions, a series of curves were made to determine the change in $4\pi M_s$ vs temperature (see Fig. 6). The 10 per cent substituted YIG was chosen as the isolator material and a shape factor was determined for this doping. An isolator was built and tested at liquid helium temperature. Table II shows comparative data for pure YIG and 10 per cent Gd-doped YIG under the conditions of a common meander line rutile loading.

Experimental Results

Gain vs Tunability

Several different meander lines were fabricated and gain vs frequency and H field mapping measurements were made. Fig. 7 shows the polarization of the RF H fields as a function of position on the meander line. Fig. 8 shows the magnitude of H^2 vs distance from the meander line surface. Note that it suggests a possible exponential decay.

Fig. 9 shows three curves of gain as a function of frequency, for three combinations of copper and air gap widths. These curves were obtained using 2.5 inches of rutile at a bath temperature of 1.7°K; in each case there was sufficient reverse isolation (greater than twice the gain) to assure no regeneration in the circuit.

Stagger tuning techniques were applied to extend the tunable bandwidth and a new set of curves was developed [5]. (See Fig. 10.) Again this data was taken for a 2.5-inch structure.

A final version of the amplifier employing 6 inches of active rutile was built. The gain as a function of frequency for this model is shown in Fig. 11. Fig. 12 shows the amplifier's reverse isolation, forward ferrite losses and total insertion losses.

Gain Stability

Sufficient reverse isolation was applied to the circuit to make this amplifier short-circuit gain stable. Data taken with an unregulated pump frequency circuit indicate both long-term and short-term stability of the amplifier to be exceptional. As an example, over a one-hour period the total variation was only ± 0.1 db, all of which could be accounted for in the variation in pump frequency and amplitude. When the amplifier was examined over a period of five minutes, the total variation was less than ± 0.05 db.

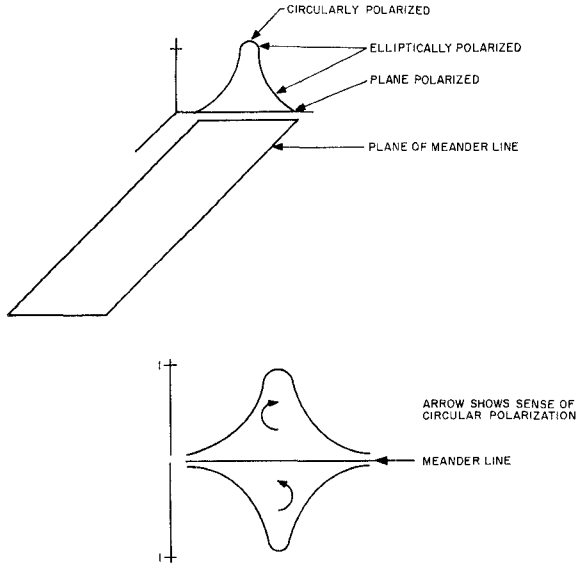

Fig. 7—Polarization of H fields above and below meander line plane.

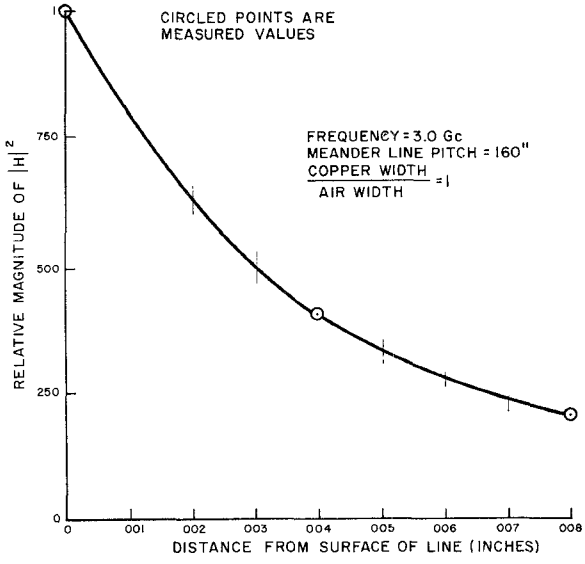

Fig. 8—Exponential decay of fields from meander line.

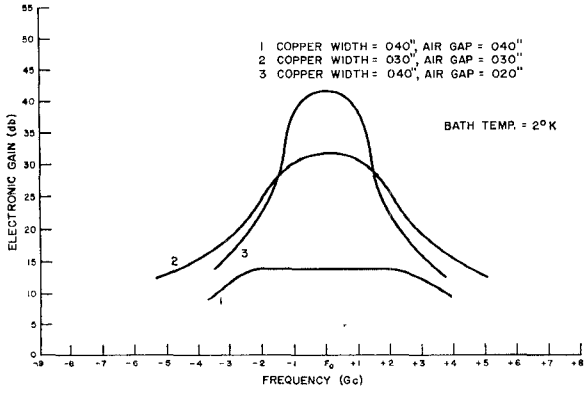

Fig. 9—Gain-vs-frequency curve for varying copper-to-air ratio.

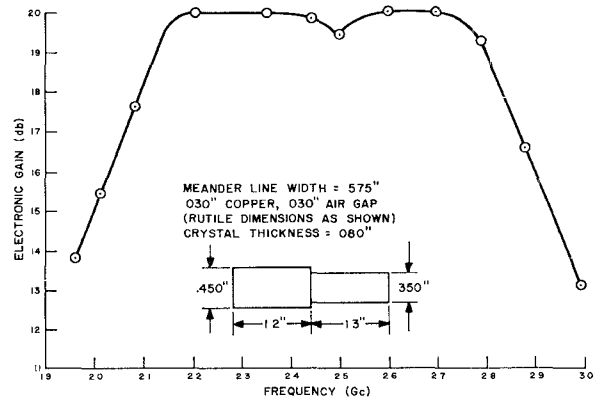

Fig. 10—Stagger-tuned experiment.

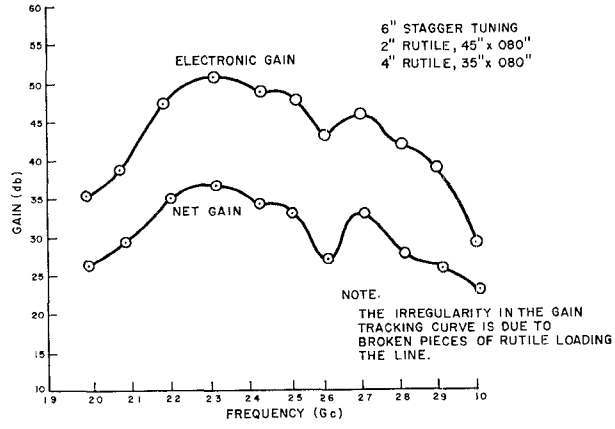

Fig. 11—Gain-vs-frequency curves for final amplifier model.

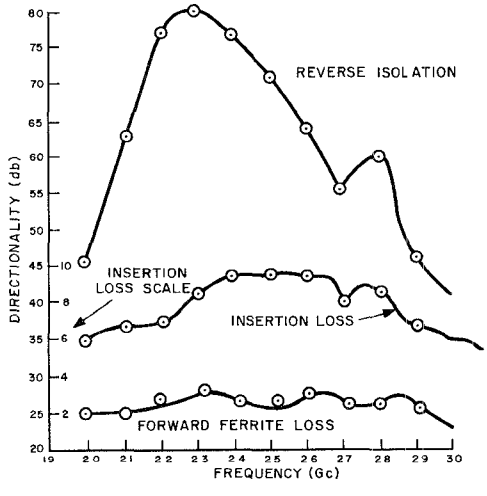

Fig. 12—Reverse isolation, ferrite losses, and total insertion losses for final amplifier model.

Bandwidth

The bandwidth and electronic gain of the amplifier were measured at a number of frequencies, and the line width computed by substitution in the equation

$$B = \Delta l \sqrt{\frac{3}{G_{\text{db}} - 3}}. \tag{5}$$

Appropriate measurements were made for a 2.5-inch structure at several frequencies and the line width was found to be a constant 31.5 Mc. After assembly of the final 6-inch structure, the measurements were repeated. Table III shows the results for a few of the points measured. The change in line width for the final structure can be attributed to the relatively poor homogeneity of the magnetic field and the multiple crystal loading of the amplifier.

Pump Power

In initial experiments with the TWM, a simple microwave cavity was used to contain the meander line circuit and the rutile and to allow the pump to couple to the rutile, as shown in Fig. 13.

At the pump frequency, the mass of rutile appears to act as a high-order mode, dielectrically loaded waveguide, with a slowing equal to $\sqrt{\epsilon}$. Unlike ruby, rutile utilizes its high dielectric constant to efficiently couple the pump energy to the crystal lattice. Accordingly, this amplifier would be expected to saturate with much less pump power than ruby (100 milliwatts) even though the relaxation times are faster. Experimental results bore this out; initial data indicated that less than 10 mw of pump power was necessary to fully saturate the crystal for 2 inches of active length.

Pump Coupling

From the Y-axis energy level curves of Fig. 2, it appears that, either the 1-3 or the 1-4 pump transition should prove suitable. This did not prove to be the case. The 1-3 pump failed; considerable effort resulted in achieving an inversion ratio of only 2:1. When the 1-4 transition was pumped, the expected 10:1 inversion ratio was observed.

On a second section of the material, X-ray back-reflection patterns were made at intervals of $\frac{3}{4}$ inch in an effort to establish the variation with direction of the c axis. The best resolution available (0.5°) limited the readings; to this accuracy there was no wandering of the c axis. Measurements were again checked at intervals of $\frac{1}{16}$ inch, and again no variation could be detected.

The inversion ratio for various chromium concentrations and bath temperatures was measured and is shown in Table IV. This inversion ratio was measured as a function of frequency, and remained fairly constant up to 5.0 Gc.

Table IV shows the optimum concentration to be approximately 0.035 per cent Cr^{+3} by weight in TiO_2 for both 1.7°K and 4.2°K operation. This inversion ratio of 10:1 was found only along the Y axis for a 1-4 pumping frequency. A complete explanation for this result is not available, since a similar experiment conducted along the crystal Z axis and X axis resulted in almost the same inversion ratios for the 1-3 and 1-4 pump transitions. A possible explanation for the Y-axis incongruity is that the 1-3 relaxation time is not equal to the 1-4 or 1-2 relaxation times, as had been expected. Fig. 14 shows a plot of pump frequency as a function of signal frequency.

TABLE III

MEASURED CHARACTERISTICS OF MASER BANDWIDTH

Frequency (Gc)	Electron Gain (db)	Measured 3 db Bandwidth Mc	Computed Line Width
2.1	38	10	34.0
2.3	42	13	43.3
2.5	42	13	43.3
2.7	38	12	41.0

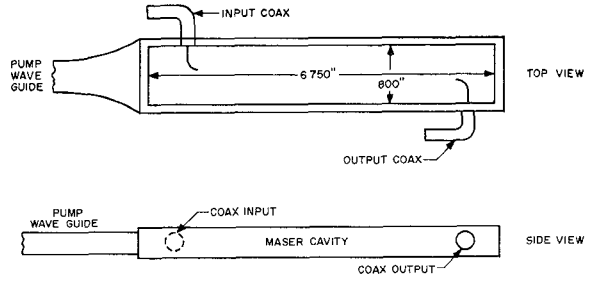

Fig. 13—Microwave cavity for TWM.

TABLE IV

INVERSION RATIO FOR VARIOUS CONCENTRATIONS AND BATH TEMPERATURES FOR Y-AXIS ORIENTATION

Cr^{+3} Concentration by Weight in TiO_2	Bath Temperature	Inversion Ratio
0.035%	1.7°K	10:1
0.035%	4.2°K	10:1
0.047%	1.7°K	7:1 to 8:1
0.093%	1.7 K	Could not invert
	4.2°K	Could not invert

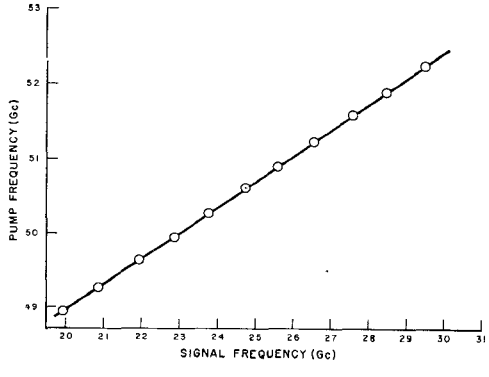

Fig. 14—Pump frequency vs signal frequency for 1-2 transition; Y-axis orientation.

Signal Saturation and Desensitization

The gain-saturation effect is shown in Fig. 15. Fig. 16 shows the gain-saturation effect of a nearby interfering signal and indicates the power level of the interfering signal required to drop the maser signal by 0.5 db. Although the saturation level of the TWM is relatively low, the dynamic range is large because of the very low noise level. It is worth noting that rutile saturates at an input level some 20 db greater than ruby.

Noise Temperature

The noise temperature of a TWM can be thought of as comprising a number of associated temperatures. The noise temperature sources include noise generated in the maser spin system, losses experienced by the forward wave (such as those in the ohmic slow wave circuit) and losses due to the input and output leads.

Within the frequency band of a given transition, the spin system acts as a noisy resistance with a noise temperature equal to the spin temperature of that transition. The spin temperature can be defined as T_s = (Bath Temperature)/(Inversion Ratio). For a maser operating at 1.7°K, the effective T_s is 0.17°K. For a bath temperature of 4.2°K, T_s has been calculated to be 0.42°K, which is the lowest reported spin temperature to date.

The noise temperature for the complete maser assembly (which does not include input and output leads) can be expressed as [13]:

$$T_a = \frac{G-1}{G}\left[\frac{a_s}{a_s - a_0} T_s + \frac{a_0}{a_s - a_0} T_0\right] \tag{6}$$

where

a_0 = Ohmic losses of slow-wave circuit, including ferrite losses.
T_0 = Bath temperature of the system.
T_s = Negative spin temperature.
a_s = Negative attenuation coefficient, or gain.

For gain to be greater than unity, of course, $a_s > a_0$, and for a good traveling-wave maser $a_s \gg a_0$ and $G \gg 1$. Under these conditions, the above equation reduces to

$$T_a = T_s + \frac{a_0}{a_s} T_0. \tag{7}$$

Since T_0 is equal to the product of T_s and the inversion ratio, T_0 and T_s are of the same order of magnitude; whereas $a_s \gg a_0$. Therefore the preceding equation can be approximated by $T_a = T_s$. In the practical case, however, the small losses before the amplifier in the input lead represent the major contribution to the system noise. The complete maser system noise temperature can then be defined as

$$T_{ms} = T_{\text{input}} + T_a + \frac{T \text{ second stage}}{\text{Gain of maser}}. \tag{8}$$

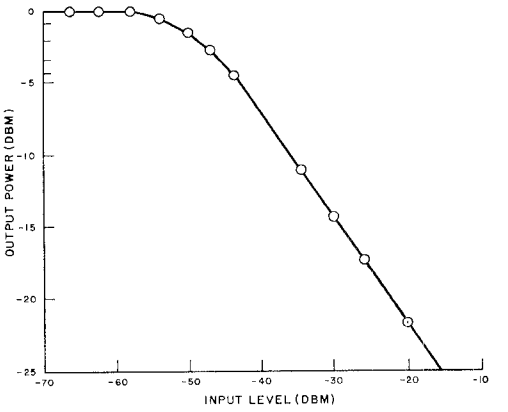

Fig. 15—Gain-saturation effect.

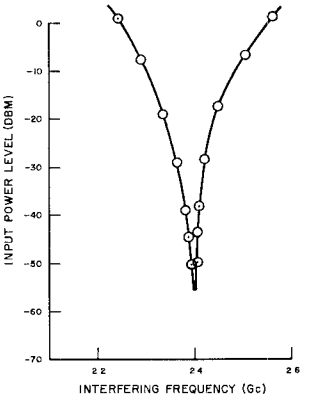

Fig. 16—Gain-saturation effect of nearby interfering signal.

The input line for the experimental model was a silver-plated, thin-walled, stainless-steel coax. Room temperature losses for this line were measured from 2.0 to 3.0 Gc for a 4-foot length; the results varied from a maximum of 0.4 db to a minimum of 0.1 db. At liquid helium temperature, the maximum value dropped to about 0.2 db, and the estimated noise contribution was 5° to 8°K. Further measurements were made to determine the noise temperature for the entire maser system; the results showed a maximum value of 8° ± 2°K, including the second stage contribution of 2.0° to 2.5°K.

Conclusions

The techniques discussed in this article and the experimental results presented have resulted in a new and improved traveling-wave maser design.

The meander line loaded with rutile demonstrates that large dielectric constant maser materials may be effectively coupled to slow-wave circuits. It should be noted that this type of maser is in its infancy and that improved performance may be accomplished by 1) Determining the proper chromium concentration and increasing the inversion ratio, 2) Loading rutile on both sides of the meander line and properly locating the rutile with respect to the surface of the line to effect an increase in the filling factor.

Many techniques for accomplishing this are now under investigation and will be reported in later articles.

ACKNOWLEDGMENT

The authors thank Dr. H. Lewis, Dr. H. Gerritsen and E. Sabisky of the RCA Laboratories in Princeton, N. J., for their many helpful discussions on the properties of rutile, and gratefully acknowledge the assistance of H. B. Yin, E. Denlinger and J. P. Laureillo with the maser measurements.

BIBLIOGRAPHY

[1] R. W. Degrasse, E. O. Schulz-Du Bois, and H. E. D. Scovil, "Three level solid state traveling-wave maser," *Bell Sys. Tech. J.*, vol. 38, pp. 305–334; March, 1959.
[2] H. D. Tenney, *et al.*, "An *S*-band traveling-wave maser," 1959, IRE WESCON CONVENTION RECORD, pt. 1, pp. 151–155.
[3] G. I. Haddad and J. E. Rowe, "*X*-band ladder-line traveling wave maser," IRE TRANS. ON MICROWAVE THEORY AND TECHNIQUES, vol. MTT-10, pp. 9–13; January, 1962.
[4] H. B. Yin, L. C. Morris, and D. J. Miller, "An *S*-band traveling-wave maser," PROC. IEEE (*Correspondence*), vol. 51, p. 225; January, 1963.
[5] D. J. Miller and H. B. Yin, "An *S*-band traveling-wave maser with a 30 per cent tunable bandwidth," PROC. IEEE (*Correspondence*) vol. 51, pp. 1779–1780; December, 1963.
[6] W. S. C. Chang, J. Cromack, and A. E. Siegman, "Cavity and Traveling Wave Masers Using Ruby at *S*-Band," Electronic Laboratories, Stanford University, Calif., Rept. No. 155-2; 1959.
[7] E. S. Sabisky and H. J. Gerritsen, "A traveling-wave maser using chromium-doped rutile," PROC. IRE (*Correspondence*), vol. 49, pp. 1329–1330; August, 1961.
[8] H. J. Gerritsen, S. E. Harrison, H. R. Lewis, and J. P. Wittke, "Chromium-doped Titania or a maser material," *Phys. Rev. Letters*, vol. 2, p. 153; 1959.
[9] E. S. Sabisky and H. J. Gerritsen, "Measurements of the dielectric constant of rutile (TiO_2) at microwave frequencies between 4.2° and 300° K," *J. Appl. Phys.*, vol. 33, pp. 1450–1453; April, 1962.
[10] P. N. Butcher, "The coupling impedance of tape structures," *J. Brit. IRE*, vol. 104, Pt. B, pp. 177–187; March, 1957.
[11] —— "A theoretical study of propagation along tape ladder lines," *J. Brit. IRE*, vol. 104, Pt. B, pp. 169–176; March, 1957.
[12] J. Clark and G. Harrison, "Miniaturized coaxial ferrite devices," *Microwave J.*, pp. 108–118; June, 1962.
[13] A. E. Siegman, Private correspondence and notes.

Coupled Circular Cylindrical Rods Between Parallel Ground Planes

EDWARD G. CRISTAL, MEMBER, IEEE

Summary—**The normalized self and mutual capacitances of periodic, circular cylindrical rods located between parallel ground planes are presented graphically. The capacitances were determined by solving the appropriate integral equation by numerical methods. Charts of self and mutual capacitance are given for rod diameter-to-ground plane spacing ratios varying from 0.05 to 0.8 and for very small to very large spacings between rods. Accuracy of the data is believed to be generally better than 2 per cent for the normalized mutual capacitance and generally better than 1 per cent for the normalized self capacitance. An approximate design method is also presented that permits using the data to synthesize filters (such as interdigital and comb-line filters) that require rods of nonequal diameters and spacings. An example of the design method is given, and a filter is constructed from the resulting data. The filter response was measured and found to agree closely with that called for by the theory.**

Manuscript received March 17, 1964. This work was sponsored by the U. S. Army Electronics Research and Development Agency, Fort Monmouth, N. J., under Contract No. DA 36-039-AMC-00084(E).

The author is with the Stanford Research Institute, Menlo Park Calif.

I. INTRODUCTION

THE DESIGN of many UHF and microwave filters is based on electrically coupling arrays of cylindrical bars located between parallel ground planes of which the comb-line and interdigital filter are two examples [1], [2]. In the past, rectangular bars generally have been used as coupling elements because the necessary data are available [3]. Filter equations and procedures of Matthaei [1], [2], together with design data of Getsinger [3], have been used to design filters which have proved to have excellent electrical characteristics. However, obtaining rectangular bars in practice requires manufacturing processes which are generally costly. On the other hand, the use of circular cylindrical rods as resonators offers several manufacturing advantages and should result in the same excellent electrical filter properties. For these reasons, design data of coupled circular cylindrical rods between parallel ground